Analytical and Bioanalytical Chemistry (2021) 413:3131–3140
https://doi.org/10.1007/s00216-021-03253-3

RESEARCH PAPER

Simultaneous electrochemical aptasensing of *patulin* and *ochratoxin A* in apple juice based on gold nanoparticles decorated black phosphorus nanomaterial

Haiyan Zhao[2] · Xiujuan Qiao[2] · Xuelian Zhang[1] · Chen Niu[1] · Tianli Yue[1] · Qinglin Sheng[1]

Received: 14 January 2021 / Revised: 23 February 2021 / Accepted: 25 February 2021 / Published online: 13 March 2021

Abstract

Simultaneous detection of patulin (PAT) and ochratoxin A (OTA) in food products is in great demand, which can prevent toxins from being exposed to human and animal bodies. However, simultaneous detection of multiple targets still faces a challenge. Herein, we developed a novel electrochemical aptasensor for the simultaneous detection of PAT and OTA in apple juice based on gold nanoparticles decorated black phosphorus (AuNPs-BP) nanomaterial. AuNPs-BP function?/work? as a sensing platform for loading much different electrochemical signal molecules functionalized aptamers. In this context, methylene blue functionalized PAT aptamers (Mb-PAT-aptamers) and ferrocene functionalized OTA aptamers (Fc-OTA-aptamers) have been introduced here to fabricate the aptasensor. Fc close to electrode surface showed a strong signal, whereas Mb was far away from electrode surface so exhibited a weak signal in the absence of OTA and PAT. Two kinds of electrochemical signal changes have been recorded dependent on target of OTA and PAT concentrations. So, simultaneous detection of OTA and PAT is achieved. Under the optimum conditions, using this developed biosensor, PAT and OTA can be quantified at a linearity range of 0.01×10^{-7} μg·mL^{-1} ~ 0.10 μg·mL^{-1}. In addition, it also has good selectivity, stability and repeatability. For the practical application, it shows promising performance for the simultaneous detection of PAT and OTA in apple juice.

Keywords Electrochemical aptasensor · Simultaneous detection · Patulin · Ochratoxin A · Apple juice

Introduction

Patulin (4-hydroxy-4H-furo (3,2c) pyran-2(6H)-one, PAT) is a toxic secondary metabolite produced by Penicillium, Aspergillus and Byssochlamys genera, et al. [1–3]. It is mainly found in fruits [1, 2, 4, 5] vegetables [2, 4] and nuts [5, 6]. Especially, it has relatively high content in rotten apples and apple juice [1]. As a result, people are easily affected by this toxic substance, causing convulsions, breathing difficulties, pulmonary congestion and other adverse effects [3, 5, 7]. The limit of PAT in apple and related products is 50.00 μg·L^{-1} in China. Similarly, ochratoxin A (OTA) is also a secondary metabolite generated by aspergillus and penicillium [8]. OTA is a very toxic contaminant in food and animal feed [9]. It widely exists in wheat [10, 11], beans [12], milk [12, 13], eggs [12, 13], wine [10, 14] and most other food products consumed by humans and animals [11, 13, 15, 16]. OTA causes varying degrees of damage to human and animal bodies, such as hepatotoxic, carcinogenic and nephrotoxic damage [10, 17]. For people and animals, contaminated foods lead to food poisoning and death in severe cases [18]. Therefore, food safety problems have become the focus of concern in the world [19]. Therefore, an increasing number of methods for the detection of these toxins have been reported, such as enzyme linked immunosorbent assay [20], fluorescence [15], liquid chromatography, colorimetric method [4, 7] and electrochemical method [21]. However, except electrochemical method, most methods have many disadvantages of long experimental period, sophisticated technique and low sensitivity.

Haiyan Zhao and Xiujuan Qiao contributed equally to this work.

✉ Tianli Yue
yuetl@nwu.edu.cn

✉ Qinglin Sheng
qlsheng@nwu.edu.cn

[1] College of Food Science and Technology, Northwest University, Xi'an 710069, Shaanxi, China

[2] College of Chemistry & Materials Science/Key Laboratory of Synthetic and Natural Functional Molecule Chemistry of Ministry of Education/Shaanxi Provincial Key Laboratory of Electroanalytical Chemistry, Northwest University, Xi'an 710069, Shaanxi, China

Given the problems mentioned above, for early prevention, simultaneous detection of multifarious food contaminants is in great request. Although electrochemical detection methods have been proven to be highly sensitive and cost-effective, simultaneous detection of multiple detection targets still meets a challenge. Compared with single-analyte method, the simultaneous assay can improve test efficiencies, lower cost, and shorter analytical procedures, et al. [22]. Thus, it is urgent to design an aptasensor for both detection of PAT and OTA quickly and sensitively.

When graphene was discovered in 2004, two-dimensional (2D) materials have been noticed in unlimited applications [23, 24]. Since then, the new synthetic techniques have been explored to prepare new-type 2D layered materials [25–29]. Recently, black phosphorus (BP), as a second fundamental single-layer nanosheet after graphene, have attracted an increasing number of attention [30] due to the availability and their two dimensionality structure [31, 32]. BP nanosheets contain phosphorus (P) atoms, in which each P atom connects to three other P atoms, leading to form a wrinkled structure with a large surface area. Compared with phosphorus allotropes of red, white and violet phosphorus, BP nanomaterials are more stable [33, 34]. Phosphorene (single layer of BP) with unique functionality can bridge the gap between graphene and transition metal oxides and transition metal dichalcogenides nanosheets in the aspect of direct bandgap and high mobility. Moreover, compared to other 2D nanomaterials, BP nanosheets exhibit the excellent biodegradability and low cytotoxicity [35]. Due to these excellent properties, BP nanosheets have been widely used in biomedical fields, such as photothermal therapy [36], biosensing [37], photodynamic therapy [38], bioimaging [39], and drug delivery [40], et al. The use of nanocomposites of gold nanoparticles and 2D materials, the nanocomposites have more advantages than the simple use of gold nanoparticles due to 2D materials' large surface area, rich bonding sites, and fast electron transfer rates. If we introduce the nanocomposites of gold nanoparticles and BP nanosheets into building electrochemical biosensor, the developed biosensor both improves the sensing platform's surface area and their sensitivity.

In this work, an aptasensor based on gold nanoparticles decorated black phosphorus (AuNPs-BP) nanomaterial was successfully fabricated. Like other two-dimensional materials, it possesses high strength and hardness, large specific surface area, tunable bandgap structure, semiconducting property, and high carrier mobility at room temperature as well as electrochemical properties [41–43]. Therefore, it can be used as a candidate of supporting materials for the proposed aptasensor. Moreover, AuNPs have been widely used in many fields due to their unique properties in recent years, such as chemical stability, excellent electronic properties, good biocompatibility, unusual catalytic and so on [44, 45]. BP and AuNPs were self-assembled to form AuNPs-BP nanocomposites, which was used to construct the proposed aptasensor for sensitively detecting PAT and OTA in apple juice simultaneously.

Experimental section

Reagents materials and samples

PAT and aflatoxin (AFB1 and AFB2) were purchased from Shanghai sangon bioengineering Co., Ltd. Ochratoxin (including OTA, OTB and OTC) was obtained from Aladdin. Black phosphorus dispersion (0.2 mg·mL^{-1}) was supplied by XFNANO (Nanjing, China). The 6-mercapto-1-hexanol (MCH) was purchased from Sigma-Aldrich. The oligonucleotides used in this work were synthesized by Takara Biotechnology Co., Ltd. And their sequences are shown in Supplementary Information Table S1. All other reagents and chemicals were of analytical reagent grade and used without further purification or treatment. Ultrapure water used in the experiment was obtained by a cartridge purification system.

Apparatus

All electrochemical experiments were carried out at the PARSTAT 3000A DX potentiostat (Princeton Applied Research) using a three-electrode system, in which a platinum wire electrode served as the auxiliary electrode, a silver-silver chloride electrode (Ag/AgCl) as the reference electrode and a modified glassy carbon electrode (PAT-cDNA & OTA-aptamer/MCH/PAT-aptamer & OTA-cDNA /AuNPs-BP/GCE) with a diameter of 3 mm was used as the working electrode. The morphologies of nanomaterials were characterized by Hitachi H-7500 transmission electron microscope (TEM). All ultraviolet-visible (UV-vis) spectra were acquired using a commercial spectrometer T6 (Beijing Purkinje General Instrument Co., Ltd., China) at room temperature. The composition of the AuNPs-BP nanocomposites was investigated by X-ray photoelectron spectroscopy (XPS, PHI 5000 Versaprobe III, Japan).

Synthesis of AuNPs-BP nanocomposites

The purchased BP dispersion (0.20 mg·mL^{-1}) was centrifuged and concentrated to 2.00 mg·mL^{-1}, and placed in the refrigerator (the temperature is 4 °C) for later use. The preparation of AuNPs mainly requires sodium citrate ($Na_3C_6H_5O_7{\cdot}2H_2O$) and chloroauric acid ($HAuCl_4$). The synthesis of AuNPs requires the following three steps: (1) 350.00 μL $HAuCl_4$ (10.00 mM) was added into 24.65 mL ultrapure water and got a homogeneous mixture solution. (2) The mixture was heated to nearly 150 °C on a heating plate. (3) 2.50 mL $Na_3C_6H_5O_7{\cdot}2H_2O$ (10.00 mM) was uniformly inject into the above solution for reacting about 25 min to get the AuNPs [46]. Under the

condition of magnetic stirring, the prepared BP dispersion (2.00 mg·mL^{-1}) and AuNPs solution were mixed at a certain volume ratio (V_{BP}:V_{AuNPs} = 3:1) and reacted for 1 h, and then obtained AuNPs-BP nanocomposites.

Preparation of sensing platform

Before modification, the glassy carbon electrode (GCE, 3 mm in diameter) was polished to a mirror-like surface with 0.05 μm alumina slurry, and washed three times by ultrapure water and ethanol-ultrapure water through ultrasonication, respectively. Then, 10.00 μL of AuNPs-BP nanomaterials were dropped onto the dried GCE, and got AuNPs-BP/GCE after drying at room temperature. Further, AuNPs-BP/GCE was incubated overnight at room temperature in a 10.00 μL 0.50 μM mixed DNA solution (containing 10.00 μM PAT-aptamers, 10.00 μM OTA-cDNA, 0.10 M Tris-HCl, pH = 7.42, and 1.00 mM TCEP). After washing with Tris-HCl buffer (pH = 7.42), the electrode was covered with 1.00 mM MCH and kept at room temperature for 1 h to block the uncovered spots of AuNPs-BP/GCE. The electrode was subsequently incubated in 10.00 μL 0.50 μM mixed solution (containing 10.00 μM PAT-cDNA, 10.00 μM OTA-aptamers, 0.10 M Tris-HCl, pH = 7.42) was added onto and then at room temperature for 2 h. Finally, the modified electrode was cleaned using 0.10 M Tris-HCl buffer (pH = 7.42). These procedure were shown in Scheme 1.

Preparation of apple samples

The fresh apples and partially rotten apples were purchased from local fruit market. Firstly, put apple slices into a juicer and mashed, the resulting paste was centrifuged and the supernatant was retained. Secondly, the supernatant of fresh apple was filtered using 0.45 μm of filter film for testing, the supernatant of partially rotten apples was filtered and further processing was required. Finally, diluted the filtered solution of partially rotten apples with 0.10 M Tris-HCl buffer (pH = 7.42) to 10 times of the original solution. It should be noted that the apple juice used for testing was freshly squeezed, and the juice of fresh apples placed at different times was kept in the refrigerator (T = 4 °C).

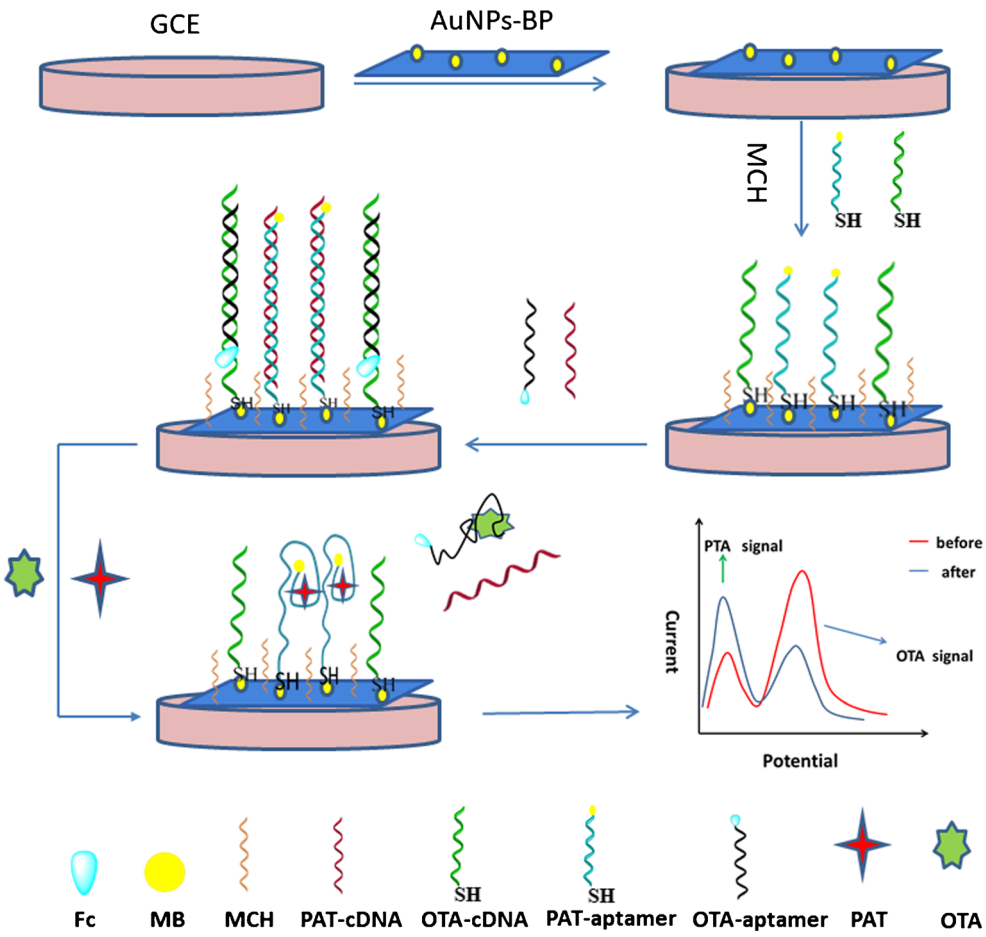

Scheme 1 The process of electrode modification and the principle of targets detection.

Results and discussion

Principle of the electrochemical aptasensor for PAT and OTA

Scheme 1 illustrates the principle of the electrochemical aptasensor for PAT and OTA. In the absence of the targets (PAT and OTA), the Mb-PAT-aptamers and Fc-OTA-aptamers hybridized with PAT-cDNA and OTA-cDNA to form double-stranded DNA (ds-DNA), respectively. The aptamers used here were chosen with the lowest K_d value (0.20 μM for OTA and 21.83 nM for PAT) and the highest binding affinity and selectivity [47, 48]. Signal of Fc closed to electrode surface showed a strong signal, whereas Mb molecule far away from electrode surface exhibited a weak signal. However, in the presence of the targets PAT and OTA, Fc-PAT-aptamers and Mb-OTA-aptamers specifically identified PAT and OTA respectively, causing PAT-cDNA and OTA-cDNA releasing to form single-stranded DNA (ss-DNA). The difference was that PAT was identified by the PAT-aptamers in electrode surface, whereas OTA-aptamers were separated from the electrode surface to identify OTA. In the presence of OTA, the OTA aptamer tended to form Fc-OTA-aptamers/OTA complex instead of the aptamer/cDNA duplex, resulting to the releasing of Fc-OTA-aptamers/OTA complex from the electrode surface and leave cDNA free again. The reason is that the affinity of OTA-aptamer/OTA complex is stronger than the combination between aptamer and cDNA [49]. So, the electrochemical signal molecule of Fc gradually decreased with the increase of OTA concentration. Similarly, when the PAT in the detection system, the aptamer specifically combined with PAT to form Mb-PAT-aptamers/PAT complex, leading to the releasing of PAT-cDNA from the electrode surface and change the aptamer structure. This is because the affinity of PAT-aptamer/PAT complex is far stronger than the combination between aptamer and partial complementary DNA fragments (pcDNA) [50]. During the process of recognizing PAT, Mb-PAT-aptamers structure changed to a curved state, resulting in the distance decrease between MB molecule and the electrode. Thus, the result is that the PAT-aptamers structure change accelerates the rate of electron transfer and the Mb signal will be enhanced.

Feasibility study on the principle of electrochemical aptasensor

The feasibility of electrochemical aptasensor was initially illustrated by electrochemical impedance spectra (EIS). The process of the proposed aptasensor test was confirmed in 5.00 mM $[Fe(CN)_6]^{3-/4-}$ solution containing 0.10 M KCl. The electron transfer resistance (R_{ct}) was described by using the Randles equivalent circuit, where C represents the double-layer capacitance, R_s represents the electrolyte solution resistance and all the connections resistance, and Z_w represents the Warburg element (insert in Fig. S2). The semicircle in EIS corresponds to the electron transfer resistance process, and the straight line represents the limited process of diffusion [51]. As shown in Fig. S2, the bare GCE showed a really small semicircle diameter in the Nyquist plots of impedance spectroscopy (GCE, 641.90 Ω, curve a). The value of semicircle diameter was minimized after the immobilization of AuNPs-BP onto the bare GCE (AuNPs-BP/GCE, 310.20 Ω, curve b) due to the good conductivity of AuNPs. When the electrode surface were modified with PAT-aptamers and OTA-cDNA, EIS exhibited a bigger interfacial resistance than the AuNPs-BP/GCE and GCE (PAT-aptamers & OTA-cDNA/AuNPs-BP/GCE, 959.50 Ω, curve c). After modifying MCH on this basis, R_{ct} further enhanced (MCH/PAT-aptamer & OTA-cDNA /AuNPs-BP/GCE, 1302.50 Ω, curve d). This was because the MCH prevented electron to transfer to modified electrode surface. The semicircle diameter further increased remarkably (1837.80 Ω, curve e) with the addition PAT-cDNA and OTA-aptamer. The electrode is defined as PAT-cDNA & OTA-aptamer /MCH/PAT-aptamer & OTA-cDNA /AuNPs-BP/GCE.

To verify the feasibility of this electrochemical sensing platform, differential pulse voltammetry (DPV) technique was applied to explain this electrochemical sensor feasibility. The electrochemical behaviors was performed in 10.00 mL of 0.10 M Tris-HCl buffer (pH = 7.42). As shown in Fig. 1, PAT-cDNA & OTA-aptamer/MCH/PAT-aptamer & OTA-cDNA /AuNPs-BP/GCE showed the original signals in the absence of OTA and PAT. It was observed that the peak currents of MB on PAT-aptamers and Fc on OTA-aptamers showed the signal at the position of - 0.2 V and 0.67 V, respectively. Fc on OTA-aptamers showed the highest current, whereas PAT-aptamers showed a lowest signal current. However, when in the presence of PAT and OTA in the detection system, the signal of Fc on OTA-aptamers decreased and MB modified PAT-aptamers increased a lot. The reason was that the combination of OTA and OTA-aptamers leave Fc-OTA-aptamers away from the electrode surface and the combination of PAT

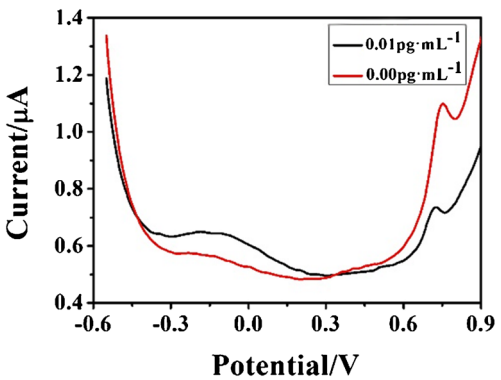

Fig. 1 The DPV of signal of the proposed aptasensor in the absence of PAT and OTA (red line) and in the presence of PAT and OTA (black line)

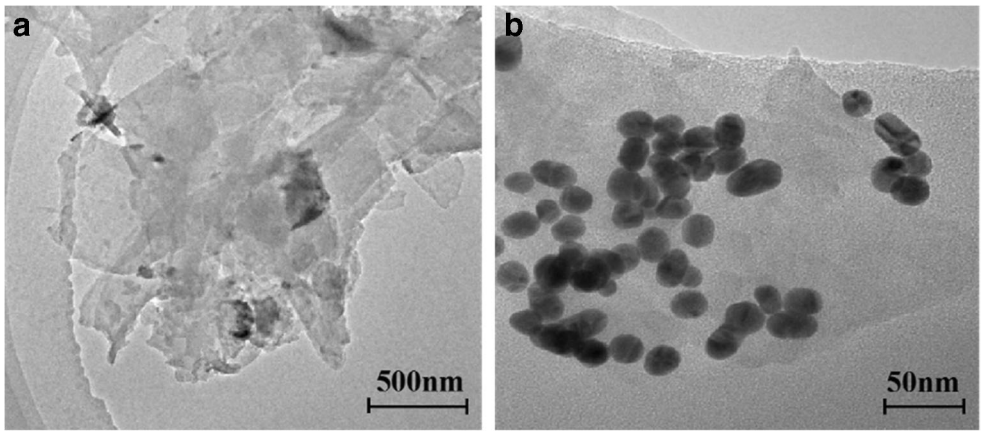

Fig. 2 TEM images of BP (a novel electrochem) and AuNPs-BP (**b**)

and PAT-aptamers led MB near the the electrode surface. Native polyacrylamide gel electrophoresis (PAGE) results were further were recorded under different conditions. In addition, the successful combination of PAT-cDNA & OTA-aptamer, PAT & PAT-aptamer, and OTA-cDNA & OTA-aptamer, OTA & OTA-aptamer have been obviously observed in Fig.S1. All results are in accordance with the mechanism diagram of this design.

Characterization of the BP and AuNPs-BP nanocomposites

TEM was employed to characterize the nanostructure structures of the BP and AuNPs-BP nanocomposites. As shown in Fig. 2a, the TEM image confirmed BP possessed a two-dimensional nanosheets structure, implying higher specific surface area for aptasensor facilitation. From Fig. 2b, it can be seen that a large number of AuNPs with a size of about 25 nm are uniformly distributed on the surface of BP, suggesting that the AuNPs-BP nanomaterial has been successfully prepared.

The compositions and chemical states of AuNPs-BP nanocomposites were investigated through the X-ray photoelectron spectra (XPS). As shown in Fig. 3a, compared to the full spectra of BP and AuNPs, the additional P and Au elements were existed in the AuNPs-BP nanocomposites, suggesting that the AuNPs-BP nanocomposites were successfully synthesized. Figure 3b and 3c showed the high resolution XPS spectra of BP before and after composite, respectively. It was found that the binding energy peaks of P were divided into two parts: (1) The peaks located near 128.80 eV and 129.50 eV corresponded to P $2p_{3/2}$ and P $2p_{1/2}$ [12, 52], respectively (Fig. 3b). The peak values of P $2p_{3/2}$ and P $2p_{1/2}$ decreased to some extent after materials hybrid when compared with BP nanosheets (Fig. 3c). (2) The peak located around 131.90 eV was indexed to POx [12, 52]. Obviously, the peak value of POx increased after materials hybrid, the possible reason is that the materials are oxidized during use. On the contrary, the peak values of Au $4f_{7/2}$ and Au $4f_{5/2}$ increased obviously after the formation of composite (Fig. 3d and 3e). The peak positions of Au $4f_{7/2}$ and Au $4f_{5/2}$ are around 83.40 eV and 87.00 eV [53, 54], respectively. The results of Au 4f showed the same trend with P 2p after materials hybrid. Ultraviolet-visible (UV-vis) spectroscopy was used to monitor the process of preparing nanocomposites. Figure 3f showed that BP exhibited a weak absorption bands at 475 nm (black curve). For AuNPs-BP nanocomposites, a strong and sharp absorption peaks at 528 nm was achieved (red curve), which belonged to the AuNPs characteristic absorption band [54, 55]. This further proved the successful preparation of the nanomaterials.

Optimization of experimental conditions

To achieve the best performance of the AuNPs-BP nanocomposites based electrochemical aptasensor, several experimental conditions including reaction time and the concentration of PAT-aptamers and OTA-cDNA were investigated. In this work, the concentration of PAT-aptamers and OTA-cDNA directly determines the response effect of electrochemical aptasensor to PAT and OTA. As indicated from Fig. S3A, the response currents changed with increasing the concentration of PAT-aptamers and OTA-cDNA from 0.20 μM to 0.80 μM, and a highest signal can be achieved when 0.50 μM of PAT-aptamers and OTA-cDNA was used. Therefore, all the following analytical studies were performed with the concentration of 0.50 μM. Meanwhile, the Fig. S3B clearly showed that with the increasing reaction time, PAT and OTA response currents increased first, then gradually stabilized. When the time reached 32 min and 24 min, the response currents of PAT and OTA reached the peak values, respectively. Therefore, the reaction time of 32 min was selected for the determination of PAT and OTA in the following experiments.

Electrochemical performance of aptasensor

Under the optimal conditions, the electrochemical behavior toward PAT and OTA in 10.00 mL of 0.10 M Tris-HCl (pH =

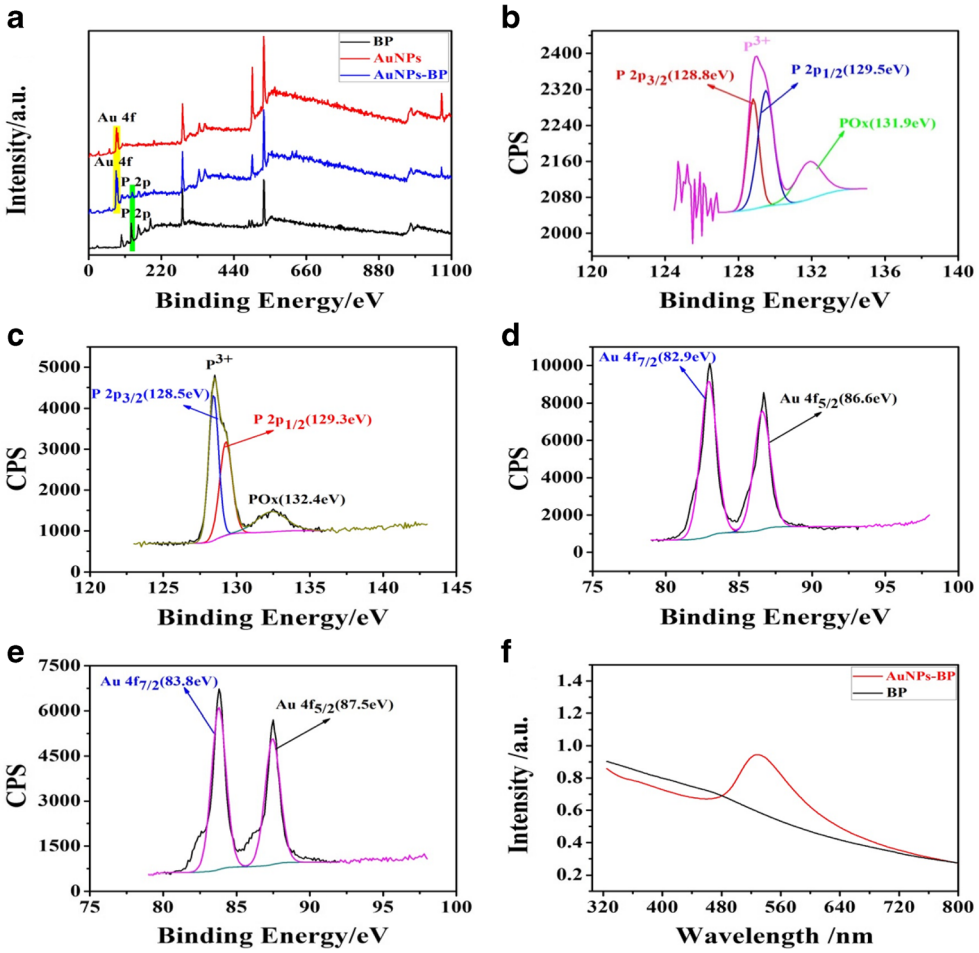

Fig. 3 The full XPS spectra of BP, AuNPs and AuNPs-BP (**a**), and the corresponding high resolutions of BP and AuNPs before and after the formation of composite (**b**-**e**). The UV-vis spectroscopy of BP and AuNPs-BP (**f**)

7.42) were assessed by differential pulse voltammetry (DPV), individually. Figure 4a showed the various responses under different PAT concentrations in the Tris-HCl buffer without OTA. It was observed that the peak currents (the current of MB) at the position of - 0.2 V increased gradually with increasing concentration of PAT (0.01×10^{-7} μg·mL^{-1} ~ 0. 10 μg·mL^{-1}). Figure 4b and 4c showed the linear regression equations between the logarithm of the concentration of PAT and the change of currents ($\triangle I = I_{target} - I_{blank}$). The linear regression equations were $\triangle I_1$ (μA) = 0.01lgC_M (pg·mL^{-1}) + 0.07 (R = 0.9996) and $\triangle I_2$ (μA) = 0.02lgC_M (pg·mL^{-1}) + 0.09 (R = 0.9927). Meanwhile, at the potential of 0.67 V (the peak position of Fc), the Fc responses gradually decreased with the increasing OTA concentration from 0.01×10^{-7} μg·mL^{-1} to 0.40 μg·mL^{-1} (Fig. 4d). In Fig. 4e and 4f, a good linear relationship can be observed between the change of differential pulse voltammetry (DPV) peak currents and the logarithm of OTA levels. The linear regression equations were $\triangle I_1$ (μA) = −0.09lgC_M (pg·mL^{-1}) - 0.68 (R = 0.9935) and $\triangle I_2$ (μA) = −0.03lgC_M (pg·mL^{-1}) - 0.69 (R = 0.9915), respectively.

The DPV experiments were performed under optimized conditions for simultaneously quantitative analysis of PAT and OTA. The peak currents of MB gradually increased with increasing concentrations of PAT, whereas the peak currents of Fc were decreased by degrees with the concentrations of OTA increased (Fig. 5a). A good linear relationship of $\triangle I$ and the logarithm of their respective concentrations have been showed in Fig. 5b ~ Fig. 5e. The linear range for simultaneous detection was determined as 0.01×10^{-7} μg·mL^{-1} ~ 0.10 μg·mL^{-1}. Compared with the separate detection results, the same linear range (0.01×10^{-7} μg·mL^{-1} ~ 0.10 μg·mL^{-1}) for simultaneous detection was obtained, respectively. The possible reasons are that the sensing platform has the poorer ability for the load of different aptamers on the same platform than loading aptamers on separate sensing platform. A comparison of this work with other aptasensors were listed in Table 1, indicating that this proposed aptasensors' performances were better than some reported literatures.

Selectivity, repeatability and stability of the aptasensor

To estimate the specificity of the proposed aptasensor, the response for PAT, OTA and different interfering substances (including AFB1, AFB2, OTB and OTC) was investigated.

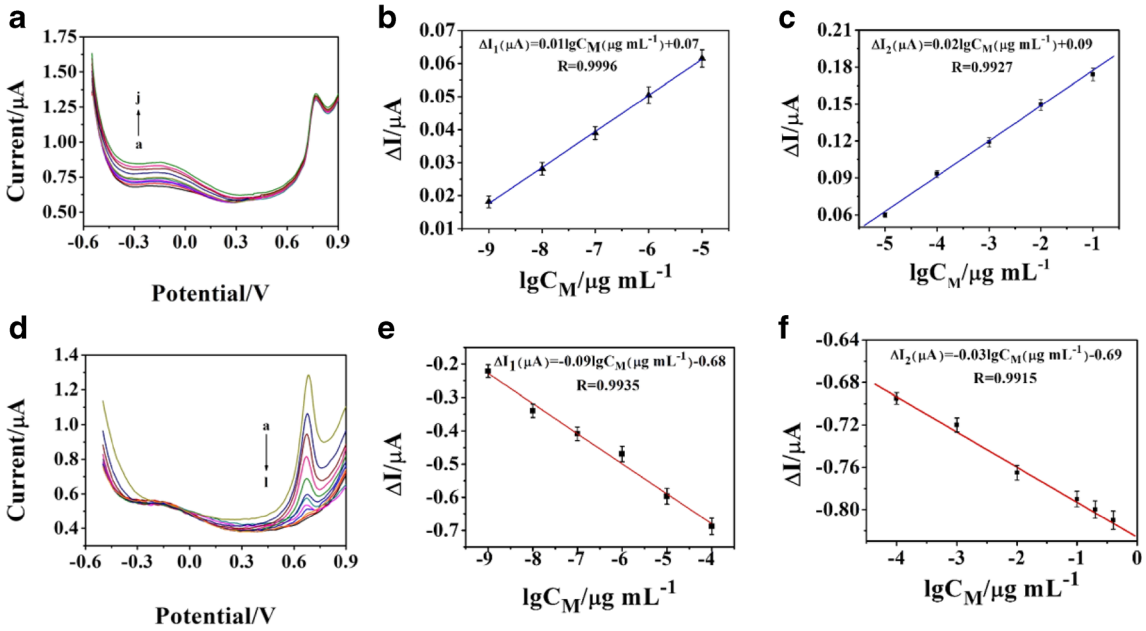

Fig. 4 DPV responses of the designed aptasensor toward PAT with different concentrations (**a** – **j**: 0.00, 0.01×10^{-7}, 0.01×10^{-6}, 0.01×10^{-5}, 0.01×10^{-4}, 0.01×10^{-3}, 0.01×10^{-2}, 0.01×10^{-1}, 0.01, 0.10 μg·mL^{-1}) in 0.10 M Tris-HCl buffer (pH = 7.42) (**a**). The linear relationship between the current increment plotted and the logarithm of concentration of PAT (**b**, **c**). DPV responses of the proposed aptasensor toward OTA with different concentrations (a - l: 0.00, 0.01×10^{-7}, 0.01×10^{-6}, 0.01×10^{-5}, 0.01×10^{-4}, 0.01×10^{-3}, 0.01×10^{-2}, 0.01×10^{-1}, 0.01, 0.10 0.20, 0.40 μg·mL^{-1}) in 0.10 M Tris-HCl buffer (pH = 7.42) (**d**). The linear relationship between the change of DPV peak current and the logarithm of OTA levels (**e**, **f**)

As shown in Fig. S4, the signal occurred in the presence of PAT and OTA. When the interfering substances with the same concentration were added in the detection system, the current values were almost no obvious change. Therefore, the proposed aptasensor has good selectivity to PAT and OTA.

Moreover, six parallel experiments were carried out to simultaneously detect PAT and OTA to evaluate the repeatability. The relative standard deviation (RSD) of PAT and OTA were 0.26% and 2.40%, respectively. The result displays a good repeatability for aptasensor. In addition, we also evaluated its stability by preserving the modified electrode at 4 °C for 21 days. The proposed aptasensor still remains more than 92.00% of the initial response signal, indicating the aptasensor possesses a satisfactory stability.

Real sample analysis

To prove the practicability of the aptasensor, the same electrochemical aptasensor was applied in the detection system for PAT and OTA detection in fresh apple juice. The detection would be carried out every 2 h. PAT and OTA contents in fresh apple juice will increased with the time going rather than no changes of their concentration. As shown in Fig. S5, with the extension of the placement time, the $\triangle I$ of the aptasensor for the response to PAT remained unchanged during the first two hours and $\triangle I$ then continuously increased with time going. $\triangle I$ of aptasensor responsing to OTA also remained unchanged for the first two hours and subsequently $\triangle I$ gradually decreased, which illustrated that the substances in the fresh

Table 1 Comparison of the analytical performances of the developed method with the reported methods

Detection method	Target	Real samples	Linear range (μg·mL^{-1})	Detection limit (μg·mL^{-1})	Reference
FRET [b]	PAT	apple juice	1.00×10^{-5}-1.00×10^{5}	0.03×10^{-4}	[6]
CD [c]	PAT	apple juice	0.50×10^{-4}-25.00×10^{-4}	0.48×10^{-4}	[7]
SWV [e]	OTA	_	1.00×10^{-9}-1.00×10^{-3}	0.03×10^{-8}	[18]
DPV	OTA	wheat QC	1.00×10^{-6}-5.00×10^{-4}	0.58×10^{-6}	[14]
DPV	OTA	wheat	0.01×10^{-3}-50.00×10^{-2}	5.60×10^{-6}	[17]
AD [f]	OTA	red wine	0.50×10^{-6}-1.00×10^{-3}	0.23×10^{-6}	[16]
DPV	PAT, OTA	apple juice	0.01×10^{-7}~0.10	–	This work

[a] high-performance liquid chromatography; [b] fluorescent resonant energy transfer; [c] colorimetric detection; [d] differential pulse voltammetry; [e] square wave pulse voltammetry; [f] amperometric detection

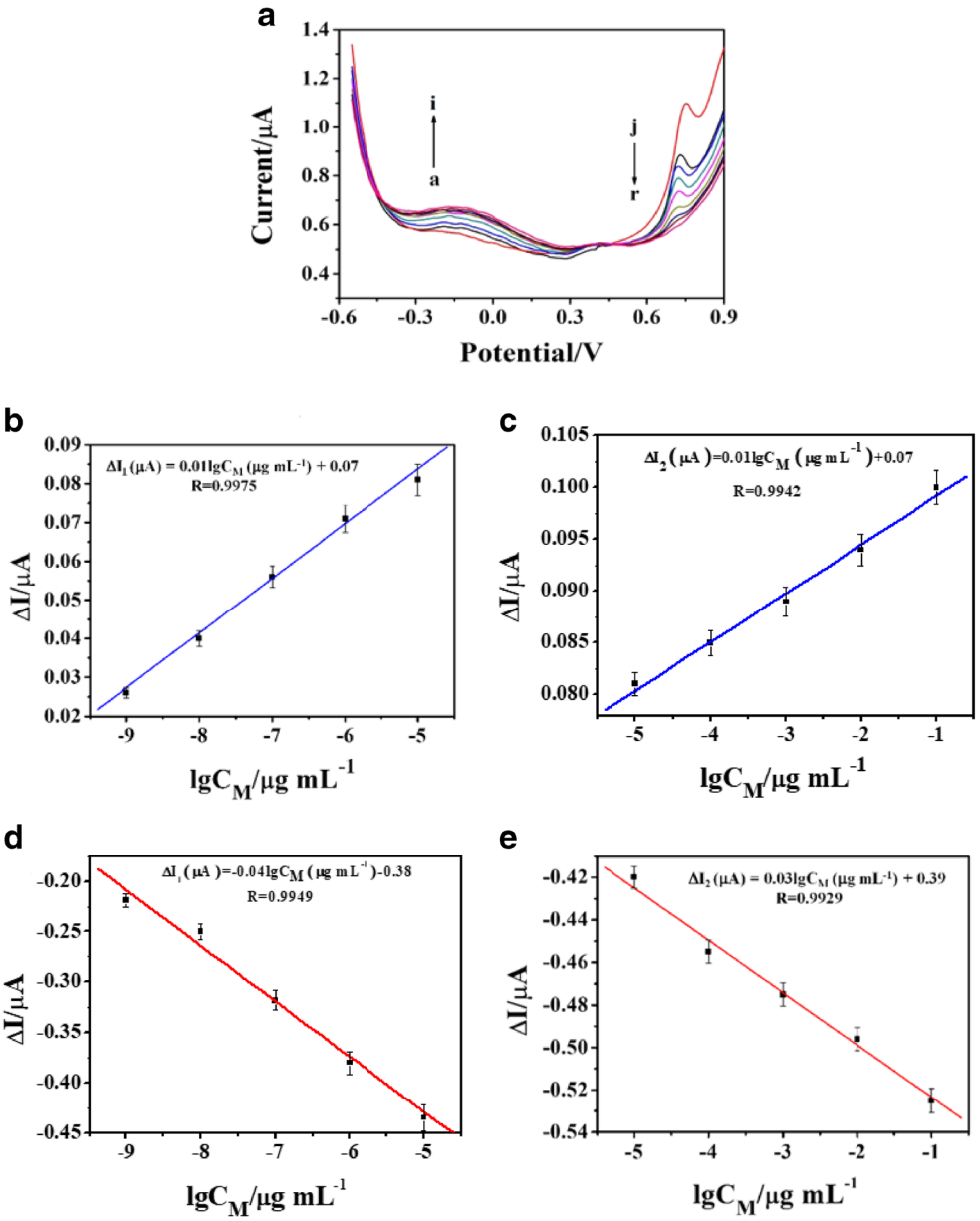

Fig. 5 DPV responses of the designed aptasensor toward PAT and OTA with concentrations of 0.00, 0.01×10^{-7}, 0.01×10^{-6}, 0.01×10^{-5}, 0.01×10^{-4}, 0.01×10^{-3}, 0.01×10^{-2}, 0.01×10^{-1}, 0.01, 0.10 μg·mL^{-1}, respectively (from a to i and from j to r, respectively) (**a**). The linear relationship between the current increment plotted and the logarithm of concentration of PAT (**b**, **c**) and the linear relationship between the change of DPV peak current and the logarithm of OTA levels (**d**, **e**)

samples could not affect the selectivity of this aptasensor. In addition, with the extension of storage time more than 2 h, the content of PAT and OTA in apple juice were constantly increasing. When the storage time reached to 10 h, the ΔI for the response to PAT and OTA significantly changed. All the results illustrated that there is no PAT and OTA in fresh apple juice within 2 h, while the concentration of PAT and OTA in fresh apple juice will occur and increase with the time going. At this point, fresh apple juice should be needed to drink in time.

In addition, the recovery studies were conducted in fresh apple juice and partially rotten apple juice by the standard addition method. The results were listed in Table S2. Fresh apple juice did not contain PAT and OTA, while partially rotten apple juice contained relatively high concentration of PAT and OTA. Recoveries of PAT and OTA are found in the range of 98.20–102.70% with RSDs from 2.60–3.84% and in the range of 100.10–104.50% with RSDs from 4.35–5.21%, respectively. Hence, the AuNPs-BP nanocomposites modified electrode can be used as an applicable material for the detection of PAT and OTA in apple juice.

Conclusion

In summary, stable and biocompatible AuNPs-BP nanocomposite was successfully synthesized. And AuNPs-BP nanocomposite based aptasensor with high specificity was constructed for simultaneous detection of PAT and OTA. Two-dimensional layered BP has a large specific surface area for

the loading of more AuNPs to further enhance the sensitivity of the aptasensor. In addition, AuNPs here connected with PAT-aptamer and OTA-cDNA through Au-S bond. Furthermore, under optimal conditions, the biosensor exhibited a wide linear range from 0.01×10^{-7} μg·mL^{-1} to 0.10 μg·mL^{-1} with good specificity, repeatability and stability. The proposed sensor was finally successfully applied to detect PAT and OTA in apple juice. The results showed expected signal responses and a satisfactory recovery. Therefore, this aptasensor has the potential to be used for PAT and OTA simultaneous analysis in foodstuffs in the future.

Supplementary Information The online version contains supplementary material available at https://doi.org/10.1007/s00216-021-03253-3.

Acknowledgments The authors gratefully acknowledge financial support from the National Key R&D Program of China (2019YFC1606703), and the Natural Science Foundation of Shaanxi Province in China (2020JM-429).

Declarations The authors declare that all experiments are in compliance with ethical standards.

Conflict of interest The authors declare that they have no competing interests.

References

1. Zhang WG, Han Y, Chen XM, Luo XL, Wang JL, Yue TL, et al. Surface molecularly imprinted polymer capped Mn-doped ZnS quantum dots as a phosphorescent nanosensor for detecting patulin in apple juice. Food Chem. 2017;232:145–54.
2. Wang XR, Jin CN, Zhong YJ, Li X, Han JH, Xue W, Wu P, Xia X.D, Peng XL. Glutathione reduction of patulin-evoked cytotoxicity in HEK293 cells by the prevention of oxidative damage and the mitochondrial apoptotic pathway. J Agr Food Chem, 2018;66:7775–7785.
3. Guo W, Pi FW, Zhang HX, Sun JD, Zhang YZ, Sun XL. A novel molecularly imprinted electrochemical sensor modified with carbon dots, chitosan, gold nanoparticles for the determination of patulin. Biosens Bioelectron. 2017;98:299–304.
4. Wu ZZ, Xu EB, Jin ZY, Irudayaraj J. An ultrasensitive aptasensor based on fluorescent resonant energy transfer and exonuclease-assisted target recycling for patulin detection. Food Chem. 2018;249:136–42.
5. Wu SJ, Duan N, Zhang WX, Zhao S, Wang ZP. Screening and development of DNA aptamers as capture probes for colorimetric detection of patulin. Anal Biochem. 2016;508:58–64.
6. Marín S, Mateo EM, Sanchis V, Valle-Algarra FM, Ramos AJ, Jiménez M. Patulin contamination in fruit derivatives, including baby food, from the Spanish market. Food Chem. 2011;124:563–8.
7. Bagheri N, Khataee A, Habibi B, Hassanzadeh J. Mimetic Ag nanoparticle/Zn-based MOF nanocomposite (AgNPs@ZnMOF) capped with molecularly imprinted polymer for the selective detection of patulin. Talanta. 2018;179:710–8.
8. Zhang Y, Yang LL, Lin CY, Guo LH, Qiu B, Lin ZY, et al. Fluorescence aptasensor for ochratoxin a in food samples based on hyperbranched rolling circle amplification. Anal Methods-UK. 2015;7:6109–13.
9. Zhang TY, Sun XF, Li L, Ma JM, Zhang RQ, Liu XL, et al. Ochratoxin a exposure impairs porcine Granulosa cell growth via the PI3K/AKT signaling pathway. Journal of Agricultural and Food Chem. 2019;67:2679–90.
10. Qing Y, Li X, Chen S, Zhou XP, Luo M, Xu X, et al. Differential pulse voltammetric ochratoxin a assay based on the use of an aptamer and hybridization chain reaction. Microchim Acta. 2017;184:863–70.
11. Liu C, Guo YJ, Luo F, Rao PF, Fu CL, Wang SY. Homogeneous electrochemical method for ochratoxin a determination based on target triggered aptamer hairpin switch and exonuclease III-assisted recycling amplification. Food Anal Method. 2017;10:1982–90.
12. Zhao Y, Zhang YH, Zhuge Z, Tang YH, Tao JW, Chen Y. Synthesis of a poly-L-lysine/black phosphorus hybrid for biosensors. Anal Chem. 2018;90:3149–55.
13. Tang J, Huang YP, Cheng Y, Huang LL, Zhuang JY, Tang DP. Two-dimensional MoS_2 as a nano-binder for ssDNA: ultrasensitive aptamer based amperometric detection of ochratoxin a. Microchim Acta. 2018;185:162.
14. Sun AL, Zhang YF, Sun GP, Wang XN, Tang DP. Homogeneous electrochemical detection of ochratoxin a in foodstuff using aptamer-graphene oxide nanosheets and DNase I-based target recycling reaction. Biosens Bioelectron. 2017;89:659–65.
15. Wang S, Zhang YJ, Pang GS, Zhang YW, Guo SJ. Tuning the aggregation/disaggregation behavior of graphene quantum dots by structure-switching aptamer for high-sensitivity fluorescent ochratoxin a sensor. Anal Chem. 2017;89:1704–9.
16. Karczmarczyk A, Baeumner AJ, Feller KH. Rapid and sensitive inhibition-based assay for the electrochemical detection of Ochratoxin a and Aflatoxin M1 in red wine and milk. Electrochim Acta. 2017;243:82–9.
17. Zhang T, Xing B, Han QZ, Lei YF, Wu D, Ren X, et al. Electrochemical immunosensor for ochratoxin a detection based on au octahedron plasmonic colloidosomes. Anal Chim Acta. 2018;1032:114–21.
18. Griffith CJ. Food safety: where from and where to? Brit Food J. 2006;108:6–15.
19. Bhat R, Rai RV, Karim AA. Mycotoxins in food and feed: present status and future concerns. Compr Rev Food Sci F. 2010;9:57–81.
20. Fernández-Baldo MA, Bertolino FA, Fernández G, Messina GA, Sanz MI, Raba J. Determination of Ochratoxin a in apples contaminated with Aspergillus ochraceus by using a microfluidic competitive immunosensor with magnetic nanoparticles. Analyst. 2011;136:2756–62.
21. Wang Z, Yu H, Han J, Xie G, Chen SP. Rare co/Fe-MOFs exhibiting high catalytic activity in electrochemical aptasensors for ultrasensitive detection of ochratoxin a. Chem Commun. 2017;53:9926–9.
22. Jiang LP, Peng JD, Yuan R, Chai YQ, Yuan YL, Bai LJ, et al. An aptasensing platform for simultaneous detection of multiple analytes based on the amplification of exonuclease-catalyzed target recycling and DNA concatemers. Analyst. 2013;138:4818.
23. Ferrari AC, Bonaccorso F, Fal'ko V, Novoselov KS, Roche S, Boggild P, Borini S, Koppens FHL, Palermo V, Pugno N, Garrido JA, Sordan R, Bianco A, Ballerini L, Prato M, Lidorikis E, Kivioja J, Marinelli C, Ryhanen T, Morpurgo A, Coleman JN, Nicolosi V, Colombo L, Fert A, Garcia-Hernandez M, Bachtold A, Schneider GF, Guinea F, Dekker C, Barbone M, Sun Z, Galiotis C, Grigorenko AN, Konstantatos G, Kis A, Katsnelson M, Vandersypen L, Loiseau A, Morandi V, Neumaier D, Treossi E, Pellegrini V, Polini M, Tredicucci A, Williams GM, Hee Hong B, Ahn J-H, Min Kim J, Zirath H, van Wees BJ, van der Zant H, Occhipinti L, Di Matteo A, Kinloch IA, Seyller T, Quesnel E,

Feng X, Teo K, Rupesinghe N, Hakonen P, Neil SRT, Tannock Q, Löfwander T, Kinaret J, Science and technology roadmap for graphene, related two-dimensional crystals, and hybrid systems. Nanoscale, 2015;7: 4598–4810.
24. Li JT, Lemme MC, Östling M. Inkjet printing of 2D layered materials. ChemPhysChem. 2014;15:3427–34.
25. Gong YJ, Lin Z, Ye GL, Shi G, Feng SM, Lei Y, et al. Tellurium-assisted low-temperature synthesis of MoS_2 and WS_2 monolayers. ACS Nano. 2015;9:11658–66.
26. Keyshar K, Gong YJ, Ye GL, Brunetto G, Zhou W, Cole DP, et al. Chemical vapor deposition of monolayer rhenium disulfide (ReS_2). Adv Mater. 2015;27:4640–8.
27. Yu J, Li J, Zhang W, Chang H. Synthesis of high quality two-dimensional materials via chemical vapor deposition. Chem Sci. 2015;6:6705–16.
28. Zhou J, Zeng Q, Lv D, Sun L, Niu L, Fu W, et al. Controlled synthesis of high-quality Monolayered α-In_2Se_3 via physical vapor deposition. Nano Lett. 2015;15:6400–5.
29. Niu L, Liu X, Cong C, Wu C, Wu D, Chang TR, et al. Controlled synthesis of organic/inorganic van der Waals solid for tunable light–matter interactions. Adv Mater. 2015;27:7800–8.
30. Li LK, Yu YJ, Ye GJ, Ge QQ, Ou XD, Wu H, et al. Black phosphorus field-effect transistors. Nature Nanotechnol. 2014;9:372–7.
31. Ren SY, Li Y, Guo QY, Peng Y, Bai JL, Ning BA, et al. Turn-on fluorometric immunosensor for diethylstilbestrol based on the use of air-stable polydopamine-functionalized black phosphorus and upconversion nanoparticles. Microchim Acta. 2018;185:429.
32. Wood JD, Wells SA, Jariwala D, Chen KS, Cho EK, Sangwan VK, et al. Effective passivation of exfoliated black phosphorus transistors against ambient degradation. Nano Lett. 2014;14:6964–70.
33. Keyes RW. The electrical properties of black phosphorus. Phys Rev. 1953;92:580.
34. Bridgman PW. Two new modifications of phosphorus. J Am Chem Soc. 1914;36:1344–63.
35. Tao W. `Zhu XB, Yu XH, Zeng XW, Xiao QL, Zhang XD, Ji XY, Wang XS, Shi JJ, Zhang H, Mei L. Black phosphorus nanosheets as a robust delivery platform for cancer theranostics Adv Mater. 2017;29:1603276.
36. Yang GC, Liu ZM, Li Y, Hou YQ, Fei XX, Su CK, et al. Facile synthesis of black phosphorus-au nanocomposites for enhanced photothermal cancer therapy and surface-enhanced Raman scattering analysis. Biomater Sci. 2017;5:2048–55.
37. Yew YT, Sofer Z, Mayorga-Martinez CC, Pumera M. Black phosphorus nanoparticles as a novel fluorescent sensing platform for nucleic acid detection. Mater Chem Front. 2017;1:1130–6.
38. Chen WS, Ouyang J, Yi XY, Xu Y, Niu CC, Zhang WY, et al. Black phosphorus nanosheets as a neuroprotective nanomedicine for neurodegenerative disorder therapy. Adv Mater. 2018;30: 1703458.
39. Xu YF, Ren F, Liu HH, Zhang H, Han YB, Liu Z, Wang WL, Sun Q, Zhao CG, Li Z, Cholesterol-modified black phosphorus nanospheres for the first NIR-II fluorescence bioimaging. ACS Appl., Mater. Inter., 2019;11: 21399–21407.
40. Qiu M, Wang D, Liang WY, Liu LP, Zhang Y, Chen X, et al. Novel concept of the smart NIR-light-controlled drug release of black phosphorus nanostructure for cancer therapy. P Natl Acad Sci USA. 2018;115:501–6.
41. Liu HW, Hu K, Yan DF, Chen R, Zou YQ, Liu HB, et al. Recent advances on black phosphorus for energy storage, catalysis, and sensor applications. Adv Mater. 2018;30:1800295.
42. Gusmão R, Sofer Z, Bouša D, Pumera M. Black phosphorus synthesis path strongly influences its delamination, chemical properties and electrochemical performance. ACS Appl Energ Mater. 2018;1: 503–9.
43. Tao W, Zhu XB, Yu XH, Zeng XW, Xiao QL, Zhang XD, et al. Black phosphorus nanosheets as a robust delivery platform for cancer theranostics. Adv Mater. 2017;29:1603276.
44. Shiraishi Y, Shirakawa E, Tanaka K, Sakamoto H, Ichikawa S, Hirai T. Spiropyran-modified gold nanoparticles: reversible size control of aggregates by UV and visible light irradiations. ACS Appl Mater Inter. 2014;6:7554–62.
45. Zhao YY, Liu RJ, Sun WY, Lv L, Guo ZJ. Ochratoxin a detection platform based on signal amplification by exonuclease III and fluorescence quenching by gold nanoparticles. Sens Actuat B-Chem. 2018;255:1640–5.
46. Su S, Zhang C, Yuwen LH, Liu XF, Wang LH, Fan CH, et al. Uniform au@ Pt core-shell nanodendrites supported on molybdenum disulfide nanosheets for the methanol oxidation reaction. Nanoscale. 2016;8:602–8.
47. Jorge AC-A, Gregory P. Determination of Ochratoxin a with a DNA Aptamer. J Agric Food Chem. 2008;56:10456–61.
48. Khan R, Aissa SB. TA. Sherazi, G. Catanante, A. Hayat, JL Marty, development of an Impedimetric Aptasensor for label free detection of Patulin in apple juice. Molecules. 2019;24:1017.
49. Yang LL, Zhang Y, Li RB, Lin CY, Guo LH, Qiu B, et al. Electrochemiluminescence biosensor for ultrasensitive determination of ochratoxin a in corn samples based on aptamer and hyperbranched rolling circle amplification. Biosens Bioelectron. 2015;70:268–74.
50. Wu ZZ, Xu EB. ZY Jin, J Irudayaraj, an ultrasensitive aptasensor based on fluorescent resonant energy transfer and exonuclease-assisted target recycling for patulin detection. Food Chem. 2018;249:136–42.
51. Zhu L, Sun Q, Xie L, Cao X. $Na_3V_2(PO_4)_3$@NC composite derived from polyaniline as cathode material for high-rate and ultralong-life sodium-ion batteries. Int J Energy Res. 2020;44:4586–94.
52. Li Q, Cen Y, Huang JY, Li XJ, Zhang H, Geng YF, et al. Zinc oxide-black phosphorus composites for ultrasensitive nitrogen dioxide sensing. Nanoscale Hori. 2018;3:525–31.
53. Su S, Cao WF, Zhang C, Han XY, Yu H, Zhu D, et al. Improving performance of MoS_2-based electrochemical sensors by decorating noble metallic nanoparticles on the surface of MoS_2 nanosheet. RSC Adv. 2016;6:76614–20.
54. Shan CS, Yang HF, Han DX, Zhang QX, Ivaska A, Niu L. Graphene/AuNPs/chitosan nanocomposites film for glucose biosensing. Biosens Bioelectron. 2010;25:1070–4.
55. Shu Y, Chen JY, Xu Q, Wei Z, Liu FP, Lu R, et al. MoS_2 nanosheet-au nanorod hybrids for highly sensitive amperometric detection of H_2O_2 in living cells. J Mater Chem B. 2017;5:1446–53.